



The effect of phase separation on crystal nucleation density and lamella growth in near-critical polyolefin blends

Go Matsuba^{*,1}, Katsumi Shimizu², Howard Wang³, Zhigang Wang⁴, Charles C. Han^{*,4}

Polymers Division, National Institute of Standards and Technology, Gaithersburg, MD, USA

Received 20 January 2004; received in revised form 13 April 2004; accepted 13 April 2004

Abstract

We have studied the effect of liquid–liquid phase separation on crystallization in near-critical blends of poly(ethylene-co-hexene)/poly(ethylene-co-octene) and poly(ethylene-co-hexene)/poly(ethylene-co-butene) using optical microscopy and simultaneous small and wide angle X-ray scattering. Two quenching schemes were used in this study: (1) single-quench, a homogeneous melt quickly cooled to the crystallization temperature, and (2) double-quench, a homogeneous melt quickly cooled to an intermediate temperature, which allows for occurring phase separation but not crystallization, then to the crystallization temperature. We could find more crystalline nuclei in case of single-quench than of double-quench. The long spacing of lamellar crystals is approximately 20 Å larger in single-quench than in double-quench, due primarily to the inclusion of more non-crystallizable components in the amorphous layers of lamellar stacks in the former. The degree of crystallinity is about three times higher in single-quench.

© 2004 Elsevier Ltd. All rights reserved.

1. Introduction

Both liquid–liquid phase separation (LLPS) and crystallization of polymers have been studied extensively during the last five decades [1–7], but studies that focus on the interplay between these two transitions are limited. Furthermore, because most previous effort has focused on determining morphologies due to the coexistence of LLPS and crystallization, the dynamical interplay during the structural development has received limited attention [8–11]. From the practical point of view, the interplay between crystallization and LLPS in polymer blends is quite

important for morphological development and mechanical properties.

A lasting interest in the polyolefin industry is synthesizing and utilizing short-chain-branched polyethylenes using metallocene catalysis, because the molecular architecture of these polyolefins can be controlled rather easily to yield homogeneous and versatile structural characteristics, such as molecular weight, molecular distribution, branching type, branching density and branching distribution [12]; as a result, broad range of morphologies and properties could be made among these linear–linear low density polyethylenes [13–15]. Because of their relatively well-defined molecular characteristics and giving more flexibility in post-synthesis design for applications, it is possible that in the blends of polyolefins, crystallinity, density, and phase-, micro- and macro-structural morphologies could be controlled with greater certainty during processing.

We have recently investigated the topics of coexisting LLPS and crystallization in copolymer blends to understand the effects of the interplay between them on structural development. We had studied the structural formation processes in the blends of poly(ethylene-co-hexene) (PEH)/poly(ethylene-co-butene) (PEB) [16–19] and PEH/poly(ethylene-co-octene) (PEOC) [20,21] by means of differential scanning calorimetry (DSC), light scattering,

* Corresponding authors. Institute for Chemical Research, Kyoto University, Gokasho, Uji Kyoto-fu 611-0011 Japan (GM). Tel.: +81-774-38-3143; fax: +81-774-38-3146.

E-mail addresses: gm@pmsci.kuicr.kyoto-u.ac.jp (G. Matsuba), c.c.han@iccas.ac.cn (C.C. Han).

¹ Institute for Chemical Research, Kyoto University, Uji, Kyoto-fu, 611-0011 Japan.

² High-throughput Factory, Harima Institute, RIKEN, Hyogo, 679-5418 Japan.

³ Department of Materials Science and Engineering, Michigan Technological University, Houghton, MI 49931, USA.

⁴ Joint Laboratory of Polymer Science and Materials, Institute of Chemistry, Chinese Academy of Sciences, Beijing, 100080, People's Republic of China.

optical microscopy, and time-resolved simultaneous small angle X-ray scattering (SAXS) and wide angle X-ray diffraction (WAXD) techniques. Both PEH/PEB and PEH/PEOC blends exhibited partial miscibility in the melt with an upper critical solution temperature (UCST), 146 °C and 172 °C, respectively. In the two-phase region above the melting temperature of polyethylene crystal (~ 125 °C), interconnected bicontinuous structural morphology, which is characteristic of the spinodal decomposition, could be observed with bright field optical microscopy (BFOM) and phase contrast optical microscopy (PCOM) [17–21]. We had studied as well the effect of amorphous component on the normalized degree of crystallinity with PEH concentration [20,21].

In this study, we focus on the effect of phase separation on crystallization of PEH/PEOC = 50/50 (denoted as HC-50) and PEH/PEB = 50/50 (HB-50) blends by mass. Inter-connected bicontinuous structures could be revealed after HC-50 annealing at 150 °C for 100 min [20,21] and HB-50 at 130 °C for 240 min [17,18], respectively. In this paper, we compare the effect of thermal history of polymer blends on crystallization, namely, crystallization from isotropic melt vs. phase separated inhomogeneous melt.

2. Experimental [22]

2.1. Sample preparation

The statistical copolymers of PEH, PEB and PEOC were synthesized using metallocene-catalysts. The PEH (weight-averaged molecular masses, $M_w = 110$ kg/mol, molecular dispersity, $M_w/M_n \sim 2$) and PEB ($M_w = 70$ kg/mol, $M_w/M_n \sim 2$) were supplied by ExxonMobil Inc. and PEOC ($M_w = 153$ kg/mol, $M_w/M_n \sim 2$) by Dow Chemical Inc. The ratios of comonomer to ethylene in PEH, PEB and PEOC are 1/57, 1/13 and 1/15, respectively. Because of lower branching content, PEH is the only crystallizable component in the blend above 60 °C. Both PEH/PEB and PEH/PEOC blends were prepared through co-precipitation method from common solutions. Equal mass of two polymers were first dissolved in a hot xylene solution at 120 °C, and stirred at 100 °C for 24 h. The solution was then quickly poured into methanol, and precipitated polymers were collected through filtering. After rinsing with excess methanol, the polymers were left dry in air for 1 day, and further dried in a vacuum oven for 72 h at the room temperature. The mixture was hot-pressed at 200 ± 2 °C to form 20 μm (for OM) thick films or 1.5 mm (for SAXS/WAXD) thick disks and quenched to room temperature.

2.2. Single and double quench

Two quenching schemes were used in this study: (1) single-quench (SQ), a homogeneous melt is quickly cooled from the initial temperature above both the equilibrium

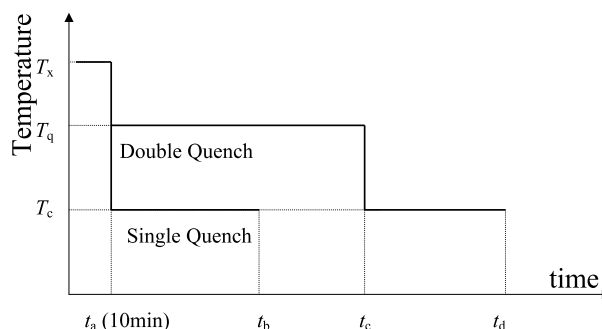


Fig. 1. Temperature condition of this paper. The rigid line indicates the temperature processes of both single and double quench conditions. For PEH/PEOC = 50/50 sample, $T_x = 200$ °C, $T_q = 142$ °C, $T_c = 119$ °C, $t_a = 10$ min, $t_b = 190$ min, $t_c = 240$ min and $t_d = 420$ min. For PEH/PEB = 50/50 sample, $T_x = 160$ °C, $T_q = 130$ °C, $T_c = 110$ °C, $t_a = 10$ min, $t_b = 190$ min, $t_c = 490$ min and $t_d = 670$ min.

melting temperature and the UCST to crystallization temperature, and (2) double-quench (DQ), a phase separated melt which is cooled from the initial homogeneous melt to between the equilibrium melting temperature and UCST is quenched to the same crystallization temperature. The thermal histories as shown in Fig. 1 were applied to both blends. For HC-50 blend, the initial melting temperature, T_x , is 200 ± 2.0 °C, the annealing temperature, T_q , 143 ± 2.0 °C, and the isothermal crystallization temperature, T_c , 119.4 ± 0.5 °C; for HB-50 blend T_x , T_q and T_c are 160 ± 2.0 °C, 130 ± 0.5 °C and 110.0 ± 0.5 °C, respectively. The sample was initially melted at 200 °C for 10 min, t_a , to eliminate the structure history. The annealing time in DQ, $t_q = t_c - t_a$, is 220 min for HC-50 or 480 min for HB-50. The isothermal crystallization time is $t_{c1} = t_b - t_a$ and $t_{c2} = t_d - t_c$ in SQ and DQ, respectively. The periods for isothermal crystallization are 180 min and 280 min for HC-50, 180 min and 230 min for HB-50, respectively.

2.3. Measurements

We carried out time-resolved SAXS, WAXD, BFOM and PCOM measurements to characterize the structure development in polymer blends with different quenching histories. The BFOM and PCOM measurements were done on a Leitz Wetzlar optical microscope with a Sony CCD camera (XC-77). A hot stage was used to control the sample temperature. Time-resolved simultaneous SAXS/WAXD measurements were performed at Advanced Polymers Beamline (X27C) at the National Synchrotron Light Source, Brookhaven National Laboratory. The wavelength of the X-ray beam was 1.366 Å with a beam size 300–400 μm in diameter at the sample position. The synchrotron X-ray beam is collimated with three 2° tapered Tantalum pinhole collimators. The SAXS/WAXD profiles were collected using position sensitive detectors (from European Molecular Biological Laboratory) with sample-to-detector distances of 1925 mm for SAXS and 110 mm for WAXD,

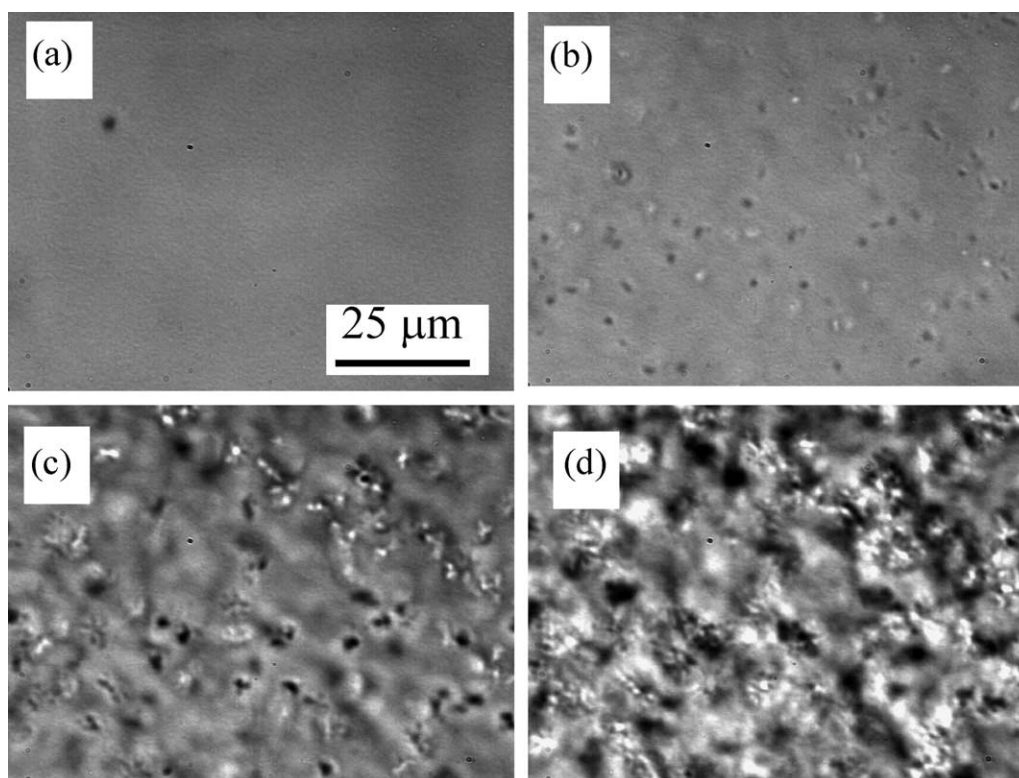


Fig. 2. Bright field optical micrographs in the single quench conditions of PEH/PEOC = 50/50 samples isothermally crystallized at 119 °C for (a) $t_{c1} = 0$ min, (b) 8 min, (c) 29 min and (d) 67 min. The scale bar in (a) is 25 μm and is the same for all pictures.

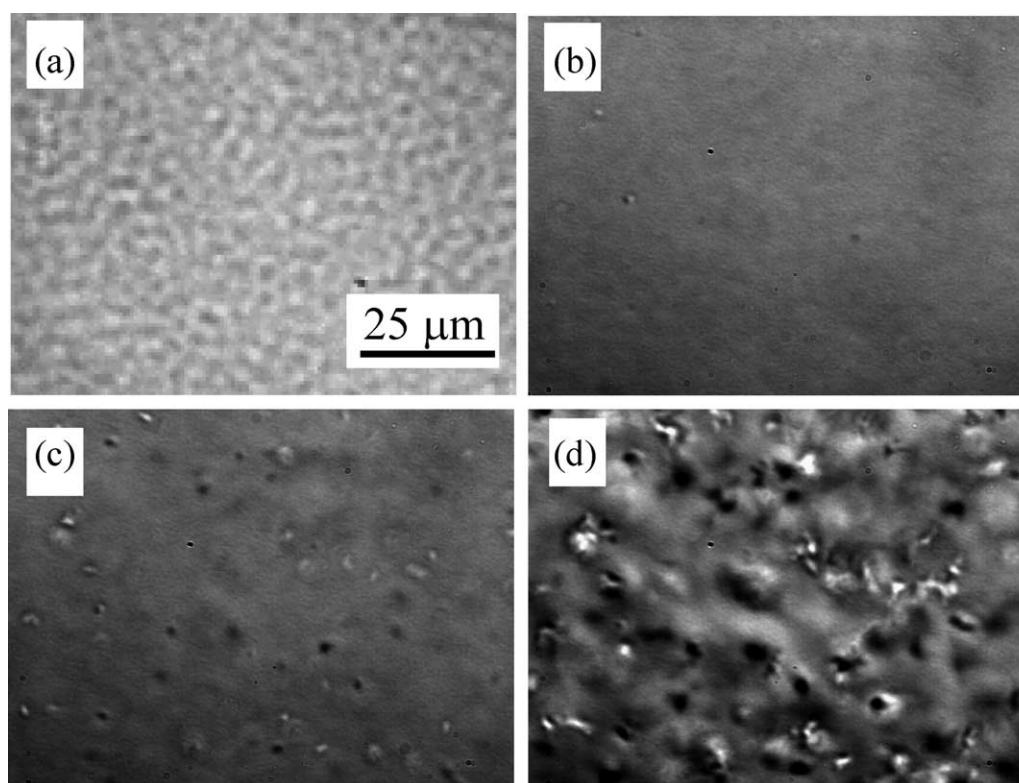


Fig. 3. (a): Phase contrast optical micrograph in the double quench condition of PEH/PEOC = 50/50 samples annealing for $t_q = 230$ min at 143 °C. (b)–(d): bright field optical micrographs after phase separation and then isothermally crystallized at 119 °C for (b) $t_{c2} = 8$ min, (c) 29 min and (d) 70 min. The scale bar in (a) is 25 μm and is the same for all figures.

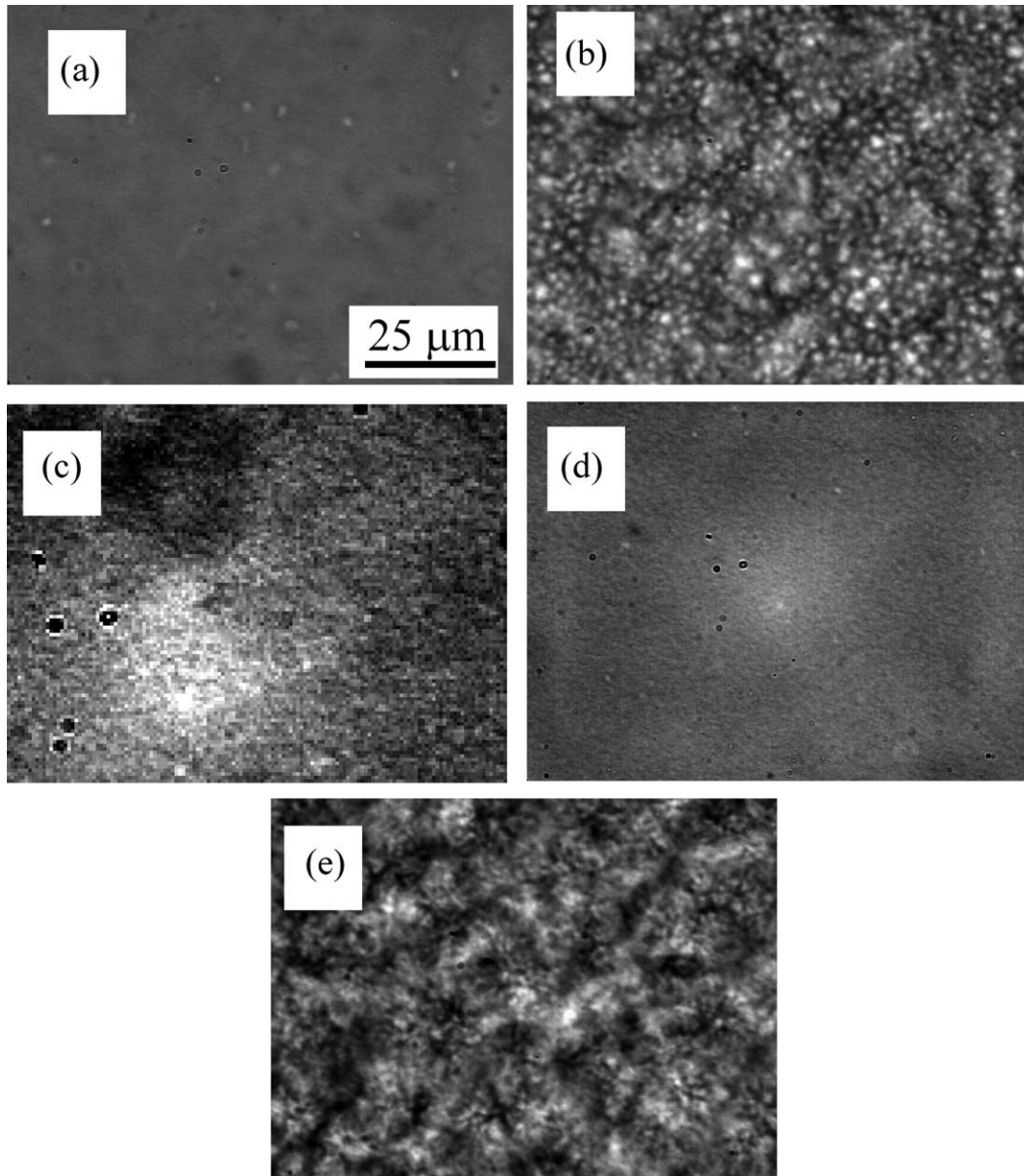


Fig. 4. Bright field optical micrographs of PEH/PEB = 50/50 samples in the single quench condition during isothermal crystallization at 110 °C for (a) 1 min and (b) 180 min. Phase contrast optical micrograph in the double quench condition annealing at 130 °C for (c) 480 min. Bright field optical micrographs in the double quench condition on isothermal crystallization at 110 °C for (d) 2 min and (e) 180 min. The scale bar in (a) is 25 μm and is the same for all figures.

respectively. The temperature jump experiments were carried out with a dual-chamber temperature apparatus, which has been described by Hsiao et al. [23,24]. The time-resolved SAXS/WAXD measurements were performed during the isothermal crystallization with a data acquisition time interval of 30 s.

3. Results

3.1. Optical microscope

Fig. 2 shows bright field optical micrographs of

HC-50 at 110 °C for crystallization time, t_{c1} , of (a) 0 min, (b) 8 min, (c) 29 min, and (d) 67 min following SQ. The scale bar in Fig. 2(a) is 25 μm and is the same for all pictures. The primary feature is due to the crystal growth of PEH component in the blend.

Fig. 3 shows the morphology of HC-50 following DQ: (a) a phase contrast micrograph annealed at 143 °C for $t_q (= t_c - t_a)$ 230 min and the bright field micrographs are isothermally crystallized at 119 °C for crystallization time, t_{c2} , of (b) 8 min, (c) 29 min, and (d) 70 min. The phase contrast microscopy is sensitive to small density fluctuations therefore used for measuring the phase morphology of LLPS, while the bright field optical microscopy is

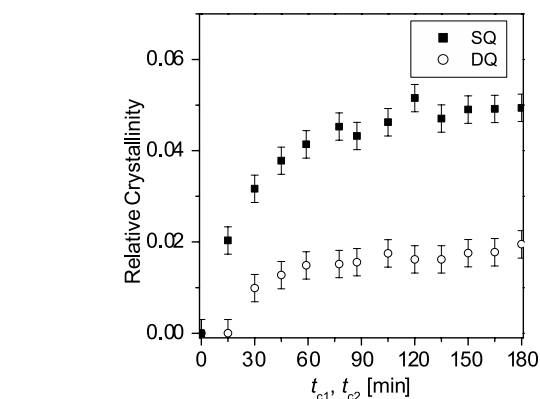
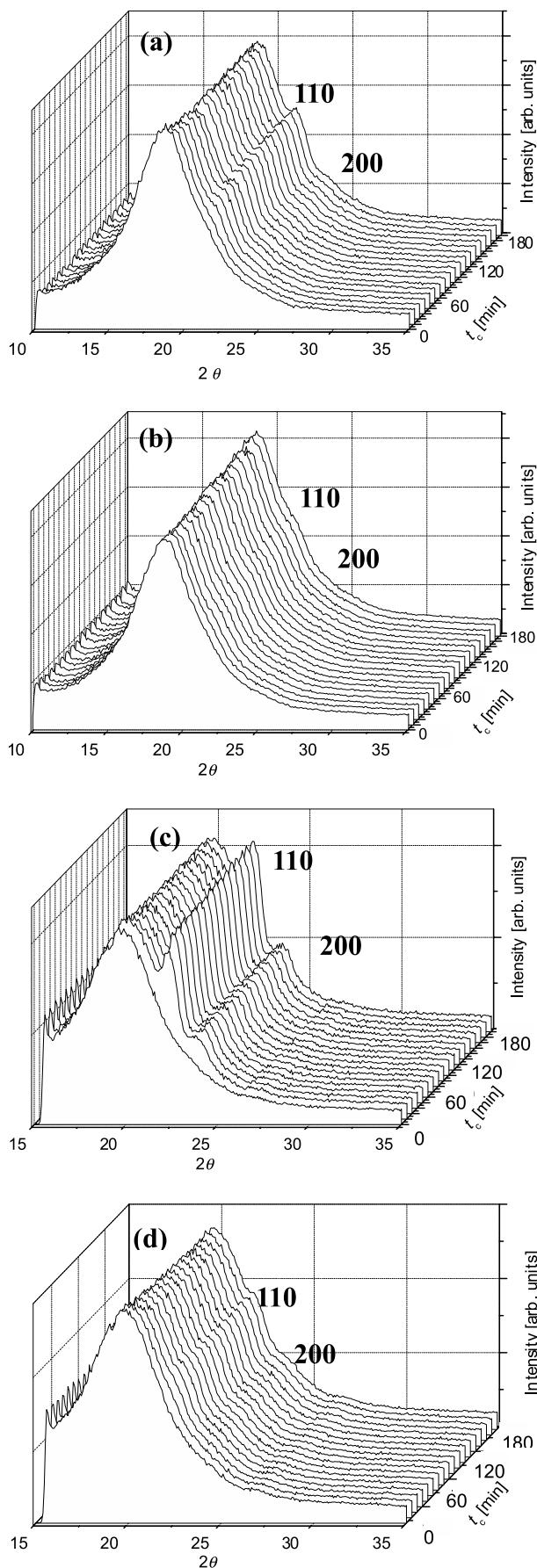


Fig. 6. The isothermal crystallization time (t_{c1} and t_{c2}) dependence of crystallinity in single and double quench for PEH/PEOC = 50/50 samples.

suitable for growth processes of spherulites. The scale bar in Fig. 3(a) is 25 μm , and is the same for all pictures.

Fig. 4(a) and (b) show the bright field micrographs of SQ morphology for HB-50 at 110 $^{\circ}\text{C}$ for $t_{c1} = 1$ min and 180 min, respectively. The DQ morphology for HB-50 are shown in Fig. 4(c), $t_q = 480$ min as revealed using PCOM, in Figs. 4(d) and (e) after $t_{c2} = 2$ min and 180 min, respectively, using BFOM. The scale bars in Fig. 4(a) is 25 μm ; and is the same for all pictures.

Bicontinuous phase structure, which is a characteristic of the late stage of spinodal decomposition, could be observed in Figs. 3(a) and 4(c). Such bicontinuous structures have been reported in PEH/PEB [16–19] and PEH/PEOC [20,21] blends in two-phase region of phase diagram. We generally find more nuclei in SQ than in DQ during the isothermal crystallization for both blends. Consequently, more spherulites are observed in SQ (Fig. 4(b)) than in DQ (Fig. 4(e)) after the isothermal crystallization for the same time at the same temperature. The density of the crystal nuclei depends on the thermal histories; hence apparently LLPS suppresses crystal nucleation resulting in more coarsened structures. However, the spherulitic growth rates of PEH/PEOC blends in both SQ and DQ are very similar about 0.03 $\mu\text{m}/\text{min}$ within error; hence the spherulitic growth kinetics is insensitive to the quenching conditions.

3.2. Simultaneous SAXS and WAXD measurements

Fig. 5 shows time-resolved WAXD profiles for (a) HC-50 at 119 $^{\circ}\text{C}$ in SQ, (b) HC-50 at 119 $^{\circ}\text{C}$ in DQ, (c) HB-50 at 110 $^{\circ}\text{C}$ in SQ and (d) HB-50 at 110 $^{\circ}\text{C}$ in DQ, respectively. At the initial times of isothermal crystallization, WAXD profiles show only amorphous halo, indicating the lack of crystalline structure prior to the temperature jump. The (110) and (200) crystal reflections

Fig. 5. The time-resolved WAXD intensity profiles of PEH/PEOC = 50/50 in (a) single quench and (b) double quench, and of PEH/PEB = 50/50 in (c) single quench and (d) double quench.

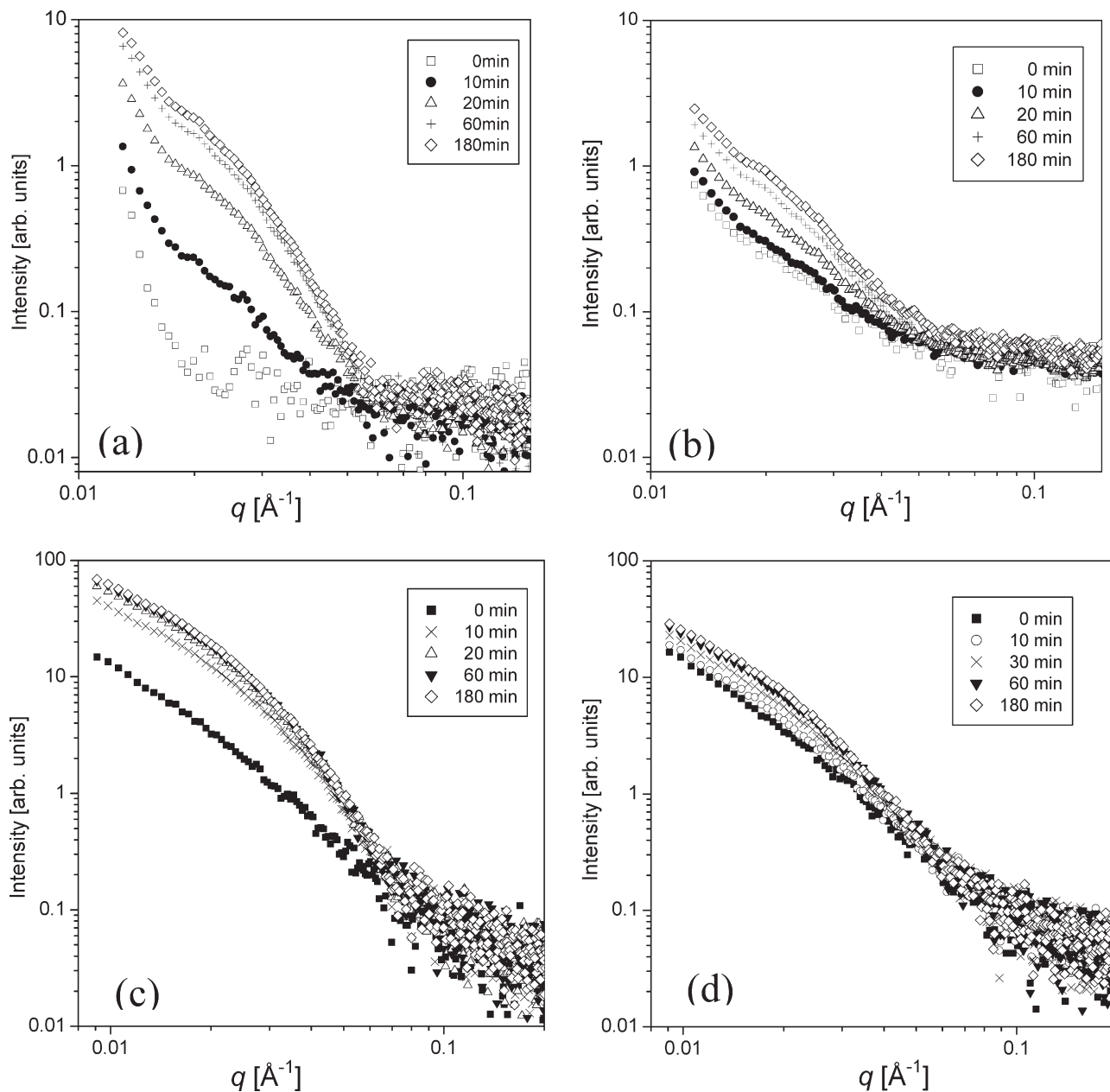


Fig. 7. The time-resolved SAXS intensity profiles of a PEH/PEOC = 50/50 blend in (a) single quench and (b) double quench, and of PEH/PEB = 50/50 in (c) single quench and (d) double quench.

develop with crystallization time, which are more prominent in SQ than in DQ for both blends. Within experimental resolution, both peak positions do not vary with the type of amorphous species, the blending composition and the annealing time, suggesting that PEH crystal lattice is not affected by blending.

For time-resolved WAXD profiles, the degree of crystallinity, X_c , can be extracted, which was detailed by Wang et al. [25]. The time evolution of X_c for HC-50 in both SQ and DQ is shown in Fig. 6, where X_c was normalized by the PEH concentration. The X_c is about $4.8 \pm 0.3\%$ for SQ and $1.6 \pm 0.3\%$ for DQ at the late stage of the isothermal crystallization.

The kinetics of crystallization follows an Avrami-like curve [26,27]. The phenomenological Avrami equation can be written as

$$1 - X_c(t_{ca}) = \exp(-kt_{ca}^n) \quad (1)$$

where, $X_c(t_{ca})$ is the crystallized weight fraction at time t_{ca} (defined as t_{c1} or t_{c2} in Fig. 1) by normalizing the $X_c(t_{ca})$ to unity at the long time limit, k is a constant depending on the nucleation and growth rates, and n is the Avrami exponent, related to the type of nucleation and growth geometry. The Avrami exponent of HC-50, n , are 1.4 for SQ and 1.7 for DQ, and then these values are similar to $n = 1.8$ in HC-50 at 114 °C for SQ [20]. The reason of larger Avrami exponent

in DQ than in SQ is that DQ crystals that grow from only PEH-rich region are better faceted. We have observed both fibrillar and isolated lamella crystal habits using atomic force microscopy in HB-50 sample [17].

Fig. 7 show the SAXS intensity as a function of the scattering vector, $q = 4\pi\sin\theta/\lambda$, where 2θ and λ are the scattering angle and the wave length of X-ray, respectively, during the isothermal crystallization for (a) HC-50 at 119 °C in SQ, (b) HC-50 at 119 °C in DQ, (c) HB-50 at 110 °C in SQ and (d) HB-50 at 110 °C in DQ, respectively. The SAXS profiles are quite different between two quenching conditions. The intensity increasing with the crystallization time in the lower q region is much larger in SQ than in DQ for both HC-50 and HB-50. This observation indicated the effect of thermal history on lamellar structure in polyolefin blends.

Fig. 8(a) and (b) show time evolution of the crystal long spacing in HC-50 as determined from SAXS profiles and the electron density correlation function derived from the SAXS profile annealed for 480 min in both SQ and DQ. The long period spacing in SQ is about 20 Å larger than in DQ as results of the inclusion of more non-crystallizable chains in amorphous layers between lamella stacks in Fig. 8(b) (SQ: 190 Å, DQ: 165 Å). During first 60 min, the

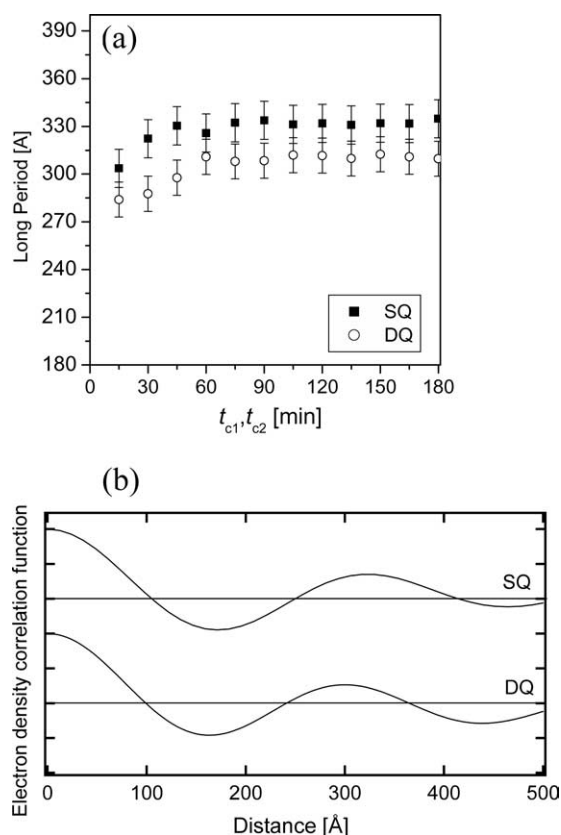


Fig. 8. (a) The isothermal crystallization time (t_{c1} and t_{c2}) dependence of long period in single and double quench of PEH/PEOC = 50/50 sample. (b) Electron density correlation functions derived from SAXS profile annealed for 480 min in SQ and DQ.

long spacing period increases with the annealing time in both SQ and DQ. This phenomena was observed just below T_m for lamella thickening which is related surface melting and re-crystallization [19–21].

4. Discussion

Generally, both crystallization kinetics and crystallinity are affected by phase morphology, although one would expect that crystallinity in phase-separated blend should be higher because the crystallizable component is already ‘purified out’ from the mixture. The experimental observations from crystallinity and nuclei density show the opposite. We pointed out that one possibility is that phase separation could suppress the co-crystallization [28–31] between the blend components. Here, we have discussed another possibility for this observation. The nucleation density could be suppressed in the separated two-phase system, resulting in smaller crystallinity. Upon phase separation, the impurities (heterogeneous structure) are most likely included in the PEH-poor phase. Moreover, we compared the crystallization half-time for both SQ and DQ from time dependence of relative crystallinity. The half-time in DQ is slightly faster than in SQ in Fig. 6 because the distance between the crystallizable PEH chains may be shorter. The SAXS intensity strength and thickness of amorphous layers, that is long spacing period, in DQ are quite smaller than that in SQ. These are due to difference of concentration for crystallizable chain on the lamella growth front between SQ and DQ. From isotropic melt, amorphous chains segregate from the lamella growth front and then gathered within lamella stacks. From phase separated melt, while PEH-rich phase is most responsible for crystallization, fewer nucleation sites cause slightly faster crystallization and smaller crystallinity in DQ in PEH-rich phase. This speculation is consistent with the optical microscopy observation by comparing Figs. 2(d) and 3(d), or Figs. 4(b) and (e). Figs. 2(d) and 4(b) show higher density crystallites in SQ, than Figs. 3(d) and 4(e) in DQ.

5. Conclusions

We have studied the effect of liquid–liquid phase separation (LLPS) on crystallization in near-critical blends of poly(ethylene-co-hexene)/poly(ethylene-co-octene) and poly(ethylene-co-hexene)/poly(ethylene-co-butene) using optical microscopy and simultaneous small and wide angle X-ray scattering. Comparing to crystallization from a previously phase separated molten blend, crystallization directly from a isotropic melt results in larger long spacing of lamellar crystals and higher crystallinity. The former is attributed to the inclusions of more non-crystallizable chains in amorphous layers of lamella stacks and the latter is due to the large nuclei density. Those results suggest that

LLPS has significant effect on the crystalline structure development in polymer blends that exhibit both transitions.

References

- [1] de Gennes PG. Scaling concepts in polymer physics. New York: Cornell University Press; 1979.
- [2] Wunderlich B. Macromolecular physics. New York: Academic; 1973.
- [3] Keller A, Cheng SZD. *Polymer* 1998;39(21):4461–87.
- [4] Cheng SZD, Keller A. *Ann Rev Mater Sci* 1998;28(21):533–62.
- [5] Otsuka N, Yang Y, Saito H, Inoue T, Takemura Y. *Polymer* 1998;39(8–9):1533–8.
- [6] Crist B, Hill MJ. *J Polym Sci, Part B: Polym Phys* 1997;35(24):2329–53.
- [7] Mandelkern L, Alamo RG, Wignall GD, Stehling EC. *Trends Polym Sci* 1996;4(11):377–83.
- [8] Morgan RL, Hill MJ, Barham PJ, Frye CJ. *Polymer* 1997;38(8):1903–9.
- [9] Rhee J, Crist B. *J Chem Phys* 1993;98(5):4174–82.
- [10] Briber RM, Khoury F. *Polymer* 1987;28(1):38–46.
- [11] Briber RM, Khoury F. *J Polym Sci, Part B: Polym Phys* 1993;31(10):1253–72.
- [12] Sehanobish K, Patel RM, Croft BA, Chum SP, Kao CI. *J Appl Polym Sci* 1994;51(5):887–94.
- [13] Bensason S, Minick J, Moet A, Chum SP, Hiltner A, Baer E. *J Polym Sci, Part B: Polym Phys* 1996;34(7):1301–15.
- [14] Chen HY, Chum SP, Hiltner A, Baer E. *J Polym Sci, Part B: Polym Phys* 2001;39(14):1578–93.
- [15] Chen HY, Chum SP, Hiltner A, Baer E. *J Appl Polym Sci* 1998;70(1):109–19.
- [16] Wang H, Shimizu K, Hobbie EK, Wang ZG, Carson-Meredith J, Karim A, Amis EJ, Hsiao BS, Hsieh ET, Han CC. *Macromolecules* 2002;35(3):1072–8.
- [17] Wang H, Shimizu K, Hobbie EK, Wang ZG, Han CC. *J Chem Phys* 2002;116(16):7311–5.
- [18] Shimizu K, Wang H, Wang ZG, Kim H, Han CC. *Abstr Pap Am Chem Soc* 2002;223:333.
- [19] Han CC, Wang H, Shimizu K, Kim H, Hobbie EK, Wang ZG. *Abstr Pap Am Chem Soc* 2002;224:761.
- [20] Matsuba G, Shimizu K, Wang H, Wang ZG, Han CC. *Abstr Pap Am Chem Soc* 2002;224:207.
- [21] Matsuba G, Shimizu K, Wang H, Wang ZG, Han CC. *Polymer* 2003;44(24):7459–65.
- [22] Certain equipment, instruments or materials are identified in the paper in order to adequately specify the experimental details. Such identification does not imply recommendation by the National Institute of Standards and Technology, nor does it imply the materials are necessarily the best available for the purpose.
- [23] Hsiao BS, Chu B, Yeh F. July 1997 NLSL Newsletter; 1. <http://nslsweb.nsls.bnl.gov/nsls/pubs/newsletters/97-jul.pdf>.
- [24] Hsiao BS, Gardner KH, Wu DQ, Chu B. *Polymer* 1993;34(19):3996–4003.
- [25] Wang ZG, Hsiao BS, Sirota EB, Agarwal P, Srinivas S. *Macromolecules* 2000;33(3):978–9.
- [26] Avrami M. *J Chem Phys* 1939;7:1103–12.
- [27] Avrami M. *J Chem Phys* 1940;8:212–24.
- [28] Kit KM, Schultz JM. *Macromolecules* 2002;35(26):9819–24.
- [29] Chen F, Shanks R, Amarasinghe G. *J Appl Polym Sci* 2001;81(9):2227–36.
- [30] Tsukame T, Ehara Y, Shimizu Y, Kutsuzawa M, Saitoh H, Shibasaki Y. *Thermochemica Acta* 1997;299(1–2):27–32.
- [31] Wignall GD, Alamo RG, Londono JD, Mandelkern L, Kim MH, Lin JS, Brown GM. *Macromolecules* 2000;33(2):551–61.